JOURNAL OF MECHANICS OF CONTINUA AND MATHEMATICAL SCIENCES
www.journalimcms.org

ISSN (Online) : 2454 -7190 Vol.-19, No.-3, March (2024) pp 22-39 ISSN (Print) 0973-8975

SIZE-DEPENDENT VIBRATION ANALYSIS OF CRACKED MICRO BEAMS REINFORCED WITH FUNCTIONALLY GRADED BORON NITRIDE NANOTUBES IN COMPOSITE STRUCTURES

L. Anitha[1], J. Sudha[2]

[1]Assistant Professor, Department of Mathematics, Nehru Memorial College Puthanampatti, Trichy, Tamilnadu, India.

[2]Assistant Professor, Department of Mathematics, Nandha Arts and Science College Erode, Tamilnadu, India.

Email : [1] anithal@nmc.ac.in, [2] sudhadeepak1212@gmail.com

Corresponding Author: **J. Sudha**

https://doi.org/10.26782/jmcms.2024.03.00002

(Received: February 02, 2024; Revised: February 24, 2024; Accepted: March 06, 2024)

Abstract

The Boron Nitride Nanotubes (BNNTs) are cylindrical nanostructures made up of nitrogen and boron atoms stacked hexagonally. Comparable to carbon nanotubes, BNNTs have exceptional mechanical, electrical, and thermal capabilities. The increasing prevalence of micro-electromechanical systems in different technological fields underscores the necessity of gaining a comprehension of their mechanical behavior. The behaviour of Functionally Graded Boron Nitride Nanotube-Reinforced Composite (FG-BNNTRC) concerning microbeam cracks during free movement is investigated in this study. BNNT can be added to a matrix of polymers in four distinct manners to give reinforcements. The BNNTRC substance features are expected by the standard of integrating fractured microbeams. This study's primary goal is to investigate the free vibration properties of FG-BNNTRC cracked micro beams. It is crucial to focus on evaluating how different BNNT reinforcing structures, volume %, dimension/thickness ratio, and length scale elements affect vibration frequencies. This paper evaluates the vibration of fractured microbeams having length dependency using the modified couple stress theory. Following examining the effects of various causes, it emerges that the frequencies exhibit noticeable variances. The study shows that when the thickness of the beam becomes closer to the length scale parameter, the size impact gets stronger. The thickness of the beam grows, and the size impact decreases. The results are significant consequences with the design in addition to developing innovative composite materials for micro-scale applications, demonstrating the details of the complex interplay among nanoscale reinforcements and structural integrity.

Keywords: Beam Theories, Boron Nitride Nanotube, Vibration, Size Effect, Functionally Graded Boron Nitride Nanotube-Reinforced Composite (FG-BNNTRC)

I. Introduction

Size-dependent vibration Analysis of Cracked Microbeams is to find out the size differences that affect how cracked microbeams vibration. Due to their small dimensions, microscale objects, including microbeams have special mechanical characteristics. The foundational strength and vibration properties are further impacted by the existence of cracks [XIV]. Cracks are one of the most significant flaws in a structure, particularly in smaller ones. A torsional spring is used to simulate cracks and the impact of these cracks on vibration systems' inherent frequencies and component lifetimes is examined. A single system crack's effects have been studied in certain studies [II]. Due to a complex interaction of elements, microbeams display unique behaviors at the microscopic scale. The goal of this work is to shed light on the intricate relationships between size-dependent vibrations in microstructures and how they influence the mechanical response of composite materials as an entire structure [XV]. Vibration-based techniques have been presented in recent decades to identify cracks in beam structures. These techniques fall into three categories: experimental, numerical, and analytical. Regardless of the approach, the most important stage that forms the foundation for further vibration analysis is fracture modeling [I]. The crack models are categorized as local flexibility models and consistent continuous cracked beam models based on the theory of fracture modeling. The local flexibility model has been utilized for vibration analysis of fractured beams. The spread of cracks results in catastrophic mishaps. To make sure that structures are reliable and secure, researchers have created numerous structural approaches for damage detection, including magnetic flux leakage, ray detection, and sonic emission [XII]. Local flexibility is a good way to define the crack that develops in the structure. The amount of flexibility will alter when a crack appears and spreads. The local crack flexibility has significant theoretical and technical significance in the identification of structural damage and can reflect the extent of the damage to the structure [XX]. Currently, the most used crack models are those that utilize the corresponding drop-section approach, the uniform crack beam theory, or local adaptability. These characteristics make Boron Nitride Nanotubes (BNNTs) attractive for use in radiation shielding, high-temperature composites like Metal Matrix Composites (MMC), transparent bulk composites, and mechanical reinforcing applications [XXVII]. Micro beams have a simple geometric shape: a straight one. For instance, knowledge has been discovered that carefully bent micro beams are appropriate for use in electrical micro relays, microvalves, micro shutter placement, and micro resonators [VI]. Since these flexed micro beams exhibit snap-through movement and vibration, they have been suggested to be employed as actuators and switches. According to a study, micro beams for micro springs or Micro-Electro-Mechanical-System (MEMS) components might be made to resemble semi-circles, serpentines, or spherical [VI]. The impact of geometrically nonlinear deformations on the nonlinear dynamic response of piezoelectric cylindrical shells reinforced with BNNTs was examined using the finite difference technique. The stability of single-walled BNNTs was investigated using a three-dimensional (3D) finite element approach The impact of tube radius on BNNT vibration frequencies, both longitudinally free and torsional [XXIII]. The study's goal is to analyze the size-dependent vibration of fractured microbeams in composite structures reinforced by FG-BNNTRC.

I.i. Key contributions

The purpose of this research is to examine broken micro beams' free vibration characteristics using an FG-BNNTRC. In addition to investigating how different length scale variables, length/thickness ratios, volume percentages, and BNNT reinforcement patterns affect vibration frequencies, this study emphasizes the importance of these findings in developing novel micro-scale composite materials by highlighting the complex relationship between structural integrity and nanoscale reinforcements.

II. Related works

The study [III] discovered each of the linear and nonlinear free vibration techniques could be used to analyze spinning two-dimensional grading micro-beams containing equal and unequal porosity distribution. The axial and thickness directions exhibit variations in the material characteristics. To monitor corrosion damage caused by chloride in reinforced concrete beams, extensive experimental research is presented in the paper [XXI]. To identify, classify, and pinpoint damage, a system that combines vibration-based monitoring with acoustic emission detection is developed. The study [XVI] provided a size dependencies are recorded in the modern constructions that have been designed and manufactured using innovative materials whose characteristics change in a continuous pattern. The work [XXII] used the simplistic elasticity method to analyze the natural fiber-reinforced composite panel having corners pointed reinforcement that is completely cracked by vibration and buckling. The work [XIX] analyzed the vibration of an Axially Functionally Graded (AFG) beam that has been post-buckled fractured. The complex differential equations are solved using an arc-length technique after being transformed into a set of algebraic equations via the Differential Quadrature (DQ) method. The study [VII] discussed Peridynamics (PD) was used to analyze the free vibration of broken plates. The numerical implementation was carried out using commercial finite element software, ANSYS, and a peridynamic Mindlin plate formulation. The paper [XXIV] examined the influence of surface and electric fields on the axial buckling of BNNTs. The outcomes are compared to the simulations of molecular dynamics to confirm that the concept of surface elasticity has been utilized effectively. The study [VIII] described a new aligned 3D epoxy/boron nitride nanosheet composite for thermal interface materials made using the radial freeze-casting technique. As a highly thermally conductive filler, hexagonal boron nitride (h-BN) has been employed in the construction of heat transport networks in polymers. The study examined the critical buckling load of a Boron Nitride Nanotube. BNNT is characterized by a higher Young's modulus, resistance to oxidation and corrosion, hardness, endurance at high temperatures, and piezoelectric and pyroelectric properties. The study [XIII] addressed the nonlocal vibration behavior of carbon/boron carbide nano-hetero-tubes in the context of a magneto-thermal atmosphere using a complex numerical model. Combining the best qualities from both architectures, hybrid nanotubes made of carbon and boron-nitride nanotubes have emerged as novel building blocks.The work

[XVII] examined the nonlinear acceleration of nanocomposite beams under transversal periodical stimulation that is seated on a nonlinear elastic basis. The study [XVIII]provided innovative functionality grading beams constructed from piezoelectric structures and carbon nanotube reinforcement composites were studied. The study [XI] provided a forced vibration analysis of a simply supported beam made of a composite material reinforced with carbon nanotubes that were exposed to a harmonic point load in the center. The single-walled carbon nanotubes are reinforced in a variety of distributions by a polymeric matrix that makes up the composite beam. The paper [IV] evaluated the free movement properties of dual beams made of single-walled functionally grading composite reinforced by significant nonmaterials. An interfacial spring holds the double beams of the construction connected. The study [XXVI] reported a straightforward, scalable, and high-throughput purification of BNNT using a modified version of the well-known sorting method known as liquid polymeric two-phase extracting. In the future, it is anticipated that the endeavor to purify BNNT on a large scale by solution purification is going to have a major role in the macroscopic realization of its outstanding features. The work [X] examined the axial buckling of BNNTs or boron nitride nanotubes. For this purpose, molecular mechanics is employed while taking into style contact that unites every atom of nitrogen and boron. The study [XXV] presented the free longitudinal vibrations of a fractured nano-beam to piezoelectric effects on the Non-Local Strained Gradient Theory (NSGT) and Euler-Bernoulli beam concept. Splitting nanoparticles into two sections and connecting these to a revolving spring serves as a model for nano-beam separation. The paper [V] examined the free vibration of a sandwich microbeam that is resting on a Winkler-Pasternak substrate and has a porous core reinforced by composite face sheets made of functionally graded carbon nanotubes. The displacement components are explained, assuming the beam is exposed to thermal stress and exists in a thermal environment.

III. The Modified Couple Stress (MCS) Theory

The enhancements made over classical couple stress theory make non-local flexibility and adapted couple stress theories more user-friendly. The energy of strain distribution is dependent on the radius of curvature tensor and the strain tensor, by the updated coupled stress theory that is put out below. Therefore, the strain energy of an isotropic linear elastic component that is stretched and filling a volume U as follows in equation (1):

$$V = \frac{1}{2}\int_U^0 \left(\sigma_{ji}\varepsilon_{ji} + n_{ji}\chi_{ji}\right) dU , \quad j, i = 1,2,3 \tag{1}$$

whereε_{ji} is the tensor of strain,σ_{ji} is the tensor of stress,χ_{ji} is the tensor of symmetric curvature, and $n_{ji}$are the elements of the combination strain tensor's deviator portion. The following is an expression for the curving matrix and strain:

$$\varepsilon_{ji} = \frac{1}{2}\left(v_{j,i} + v_{i,j}\right) \tag{2}$$

$$\chi_{ji} = \frac{1}{2}\left(\theta_{j,i} + \theta_{i,j}\right) \tag{3}$$

Where θ_i are the elements that make up the rotation vector, which is described as $v_j$are the elements that comprise the vector of displacement.

$$\theta_{j,i} = -\frac{1}{2} f_{jil} v_{l,i} \tag{4}$$

whichf_{jil}represents a combination. The fundamental connections are represented as follows equation (5) and (6):

$$\sigma_{ji} = \lambda \varepsilon_{ll} \delta_{ji} + 2\mu \varepsilon_{ji} \tag{5}$$

$$n_{ji} = 2\mu k^2 \chi_{ji} \tag{6}$$

where$\delta_{ji}$is the delta of Kronecker and $2k^2$is definite as k^2 , λindicates the influence of the combination force and represents an element longitudinal scaling factor. In addition, Lame's constants, $\lambda$and μ, have the following definitions:

$$\lambda = \frac{Fu}{(1+u)(1-2u)}, \mu = \frac{F}{2(1+u)} \tag{7}$$

The shear modulus (μ) and the Poisson's ratio (PR) (u) are represented in the given formulae.

III. i. Model of a cracked micro-beam

In this paradigm, the cracked and untracked parts of a beam are seen as two distinct entities. It is believed that the part without cracks will bear the brunt of the weight, while the cracked part is considered an independent element with weaker rigidity and strength. Using this method, engineers may determine if a beam with pre-existing cracks is structurally sound and how it will react to different loads. Examining the beam revealed that it contains an edge fracture of length a, located $K^d$from the left end. To manage the extra strain energy produced on the crack, springing is included. A potential method to express the strain power generated by the microbeam as an effect is as follows:

$$\Psi = \frac{1}{2} \int_0^K dw \int_B^0 \sigma_{ww} \left(\frac{\partial v}{\partial w} - z \frac{\partial^2 x}{\partial w^2} \right) dB + \Delta\Psi_d \tag{8}$$

$\Delta\Psi_d$is the further energy produced by a fracture in strain. Regarding the longitudinal force and the bending moment, the formula could be expressed as follows:

$$\Psi = \frac{1}{2} \int_0^K dw \int_B^0 \sigma_{ww} \left(\frac{\partial v}{\partial w} - z \frac{\partial^2 x}{\partial w^2} \right) dB + \Delta\Psi_d \tag{9}$$

The increase brought an edge crack has the following expression:

$$\Delta\Psi_d = \frac{1}{2} l_{NN} N(K^l, s) \frac{\partial^2 x}{\partial w^2} + \frac{1}{2} l_{MM} M(K^l, s) \frac{\partial v}{\partial w} + \frac{1}{2} l_{NM} N(K^l, s) \frac{\partial v}{\partial w} + \frac{1}{2} l_{MN} M(K^l, s) \frac{\partial^2 x}{\partial w^2} \tag{10}$$

which stand for the adaptability constants $l_{NN} l_{MM} l_{NM} l_{MN}$. The related impacts involving axial force and moment of bending have been taken into consideration by considering the final pair of terms.

$$\Delta\Psi_d = \frac{1}{2} N\Delta\theta + \frac{1}{2} M\Delta v \tag{11}$$

The proportional horizontal movement at the edge crack section is represented by Δv, whereas $\Delta\theta$ represents the angle rotated by the rotating spring. Δvas well as$\Delta\theta$ can be expressed as:

$$\Delta\theta = l_{NN}\frac{\partial^2 x}{\partial w^2} + l_{NM}\frac{\partial v}{\partial w} \tag{12}$$

$$\Delta v = l_{MM}\frac{\partial v}{\partial w} + l_{MN}\frac{\partial^2 x}{\partial w^2} \tag{13}$$

Since the focus of this inquiry is transverse free vibrations, transverse movement is not taken into account. Furthermore, it is commonly believed that the adaptability constants$l_{NN} l_{NM} l_{MM} and l_{MN}$are compact, meaning that the smallest constantl_{MM}, which is connected to the bending moment, is taken into account. Utilizing dimensionless variables, the slope increment $\Delta\theta$ in the fractured portion is stated as follows:

$$\Delta\theta = \frac{l_{NN}}{K}\frac{\partial^2 \bar{X}}{\partial w^2}\Big|_{\xi=K^d} = L\frac{\partial^2 \bar{X}}{\partial w^2}\Big|_{\xi=K^d} \tag{14}$$

Following the definition of the crack beam model, each of the two segments may be subjected to the calculation for movement in the direction that is vertical to begin the study of the beam's free transverse vibration:

$$\bar{U}^{(4)}(\xi) + n^2 r^4 \lambda^4 \bar{U}''(\xi) - r^4 \lambda^4 \bar{U}(\xi) = 0,\ \ 0 \le \xi \le a \tag{15}$$

$$\bar{U}^{(4)}(\xi) + n^2 r^4 \lambda^4 \bar{U}''(\xi) - r^4 \lambda^4 \bar{U}(\xi) = 0,\ \ a \le \xi \le 1 \tag{16}$$

where the normal frequencies component is denoted by λ^4. For every section, the general solution may be expressed as follows:

$$\bar{U}(\xi) = B_1 sing(\beta_q \xi) + B_2 cosg(\beta_q \xi) + B_3 \sin(\beta_j \xi) + B_4 \cos(\beta_j \xi),\quad 0 \le \xi \le a$$

$$\bar{U}(\xi) = A_1 sing(\beta_q \xi) + A_2 cosg(\beta_q \xi) + A_3 \sin(\beta_j \xi) + A_4 \cos(\beta_j \xi),\quad a \le \xi \le 1 \tag{17}$$

$$\bar{U}_2(a) = U_1(a) \tag{18}$$

Each of the eight unexplained variables in the equations mentioned above and calculated by using the transition restrictions as well as the additional compatible requirements listed at the portion that is cracked: how consistent with what the horizontal movement is,

$$\bar{U}_2'(a) - \bar{U}_1'(a) = L\bar{U}_1''(a) \tag{19}$$

the bending moment's continuity,

$$\bar{U}_2''(a) = \bar{U}_1''(a) \tag{20}$$

the shear force's continuous,

$$\bar{U}_2'''(a) = \bar{U}_1'''(a) \tag{21}$$

A linear system of equations is produced by setting the previously specified conditions and the basic support boundary conditions into Equation (17). The design should be emphasized since this is a homogeneous system. The organization regarding the elements' matrix's variables, which represent the basic frequency.

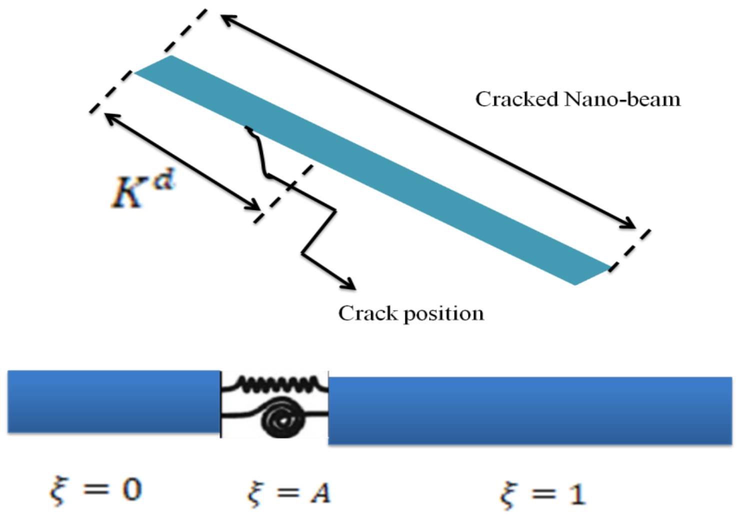

Fig 1. Diagram of a microbeam crack

III.ii Developing the problem

A microbeam, as shown in Figure 1 has the following dimensions: breadth$b$, length$L$, and height h. A rotating spring at the fracture location and a longitude are used to represent the microbeam's crack. The micro beams' unrestricted transversal is taken into account. The principle developed by Hamilton to be used for calculating the governing equations. The movement of the vector across the direction of the beam at any given location might be written as follows, according to the Euler-Bernoulli beam theory:

$$v_w(w,y,s) = -y\frac{\partial x(w,s)}{\partial w} \tag{22}$$

$$v_z(w,y,s) = 0 \tag{23}$$

$$v_y(w,y,s) = x(w,s) \tag{24}$$

where$s$ represents time and $v$is the beam's transverse displacement measured along its neutral axis at any point.

$$\varepsilon_{ww} = -y\frac{\partial^2 x(w,s)}{\partial w^2} \tag{25}$$

Furthermore, when Equation (8) is substituted into Equation (4), the sole nonzero component results is:

$$\theta_z = -\frac{\partial x(w,s)}{\partial w} \tag{26}$$

Moreover, the curvature tensor components of Equation (3) will be expressed as follows once the above equation is substituted:

$$\chi_{wz} = -\frac{1}{2}\frac{\partial^2 x(w,s)}{\partial w^2} \tag{27}$$

$$\chi_{ww} = \chi_{zz} = \chi_{yy} = \chi_{wy} = \chi_{zy} = 0 \tag{28}$$

Equations (1) and (29) can be used to express the prospective potential of the microbeams utilizing the adapted couple stress concept.

$$V_{SE} = \frac{1}{2}\int_0^K \left(\frac{F(1-u)J}{(1+u)(1-2u)} + \frac{1}{2}\mu Bk^2\right)\left(\frac{\partial^2 x(w,s)}{\partial w^2}\right)^2 dw \tag{29}$$

Conversely, the beam's kinetic energy may be determined as follows:

$$U = \frac{1}{2}\int_0^K \left[\rho B\left(\frac{\partial x(w,s)}{\partial s}\right)^2 + \rho\left(\frac{\partial^2 x(w,s)}{\partial w\partial s}\right)^2\right] dw \tag{30}$$

where ρ represents the beam's frequency. Therefore, the problem's Lagrangian functional can be expressed as follows:

$$K = U - V_{SE} \tag{31}$$

Therefore, Hamilton's concept produces the following regulating solution and boundary circumstances:

$$\delta\int_0^S K ds = 0 \tag{32}$$

Using the functional initial variation as a calculation

$$\int_0^S\int_0^K (\rho B\frac{\partial w}{\partial s}\frac{\partial\delta x}{\partial s} + \rho J\frac{\partial^2 w}{\partial w\partial s}\frac{\partial^2\delta x}{\partial w\partial s} - \left(\frac{F(1-u)J}{(1+u)(1-2u)} + \frac{1}{2}\mu Bk^2\right)\frac{\partial^2 x}{\partial w^2}\frac{\partial^2\delta x}{\partial w^2})\, dwds = 0 \tag{33}$$

Coefficients of dw will be adjusted to zero by integrating Equation (33) by portions while keeping in mind the fundamental lemma of the calculus of variations.

$$\left(\frac{EI(1-u)}{(1+u)(1-2u)} + \frac{1}{2}\mu Bk^2\right)\frac{\partial^4 x(w,s)}{\partial w^4} + \rho B\frac{\partial^2 x(w,s)}{\partial s^2} - \rho J\frac{\partial^2 x(w,s)}{\partial w^2\partial s^2} = 0 \tag{34}$$

Additionally, the conditions for the boundary of the beam at its edges$k(w = 0 \quad w = K)$could be expressed as follows:

$$Either\left(\frac{EI(1-u)}{(1-u)(1-2u)} + \frac{1}{2}\mu Bk^2\right)\frac{\partial^3 x(w,s)}{\partial w^3} + \rho J\frac{\partial^3 x(w,s)}{\partial w\partial s^2} = 0 \quad x = 0$$

$$Either\left(\frac{EI(1-u)}{(1-u)(1-2u)} + \frac{1}{2}\mu Bk^2\right)\frac{\partial^3 x(w,s)}{\partial w^2} = 0 \quad \frac{\partial^2 x(w,s)}{\partial w^2} = 0 \tag{35}$$

where the mass moments of gravity of the beam is represented by ρJ and the stiffness of flexion by EI.

Equation (34) can have its steady-state solution expressed as $x(w,s) = U(w)f^{j\Omega s}$. By inserting the expression $U(w)f^{j\Omega s}$into Equation (34) can be expressed as follows since the time variable will be removed:

$$\left(\frac{Ei(1-u)}{(1-u)(1-2u)} + \frac{1}{2}\mu Bk^2\right)U^{(4)}(w) + \rho J\Omega^2 U''(w) - \rho B\Omega^2 U(w) = 0 \tag{36}$$

where$w$ and double prime symbol, respectively, represent the additional derivatives relative to vibration frequency w, and Ω indicates the 2nd derivative about w. Assuming variable constants and dimension elements as follows:

$$\overline{U} = \frac{U}{K}, \xi = \frac{w}{K}, \lambda^4 = \frac{\rho BK^4\Omega^2}{EI} \tag{37}$$

By using Equation (37) in place of (36), the transverse free vibration may be written as follows:

$$\overline{U}^{(4)}(\xi) + n^2 r^4 \lambda^4 U''(\xi) - r^4 \lambda^4 U(\xi) = 0 \tag{38}$$

where

$$r^4 = \frac{EI}{\frac{EI(1-u)}{(1+u)(1-2u)} + \frac{1}{2}\mu B k^2}, n^2 = \frac{1}{K^2 B} \tag{39}$$

It requires to be remembered that A is the beam's cross-sectional area. The overall solution is derived as follows by calculating the differential Equation (38) and locating the source of the associated characteristic equation:

$$U(\xi) = B_1 sing(\beta_q \xi) + B_2 cosg(\beta_q \xi) + B_3 sin(\beta_j \xi) + B_4 cos(\beta_j \xi) \tag{40}$$

whereβ_q and β_j are:

$$\beta_q = r\lambda \left(\frac{n^4 r^4 \lambda^4 + 4 - n^2 r^2 \lambda^2}{2}\right)^{1/2}$$

$$\beta_q = r\lambda \left(\frac{n^4 r^4 \lambda^4 + 4 + n^2 r^2 \lambda^2}{2}\right)^{1/2} \tag{41}$$

III.iii. Boron nitride nanotube-reinforced nanocomposite plate using Eshelby–Mori–Tanaka approach

Nanotubes composed of boron and nitrogen atoms organized in a hexagonal lattice have unique features compared to carbon nanotubes. These cylindrical structures resemble carbon nanotubes. The mechanical, thermal, and electrical properties of a nanocomposite plate are improved by incorporating these BNNTs into the matrix material, which is a polymer or a ceramic. Unique properties, such as high heat conductivity, extraordinary strength, and endurance to high temperatures are impacted by the inclusion of BNNTs. The Eshelby-Mori-Tanaka method, which determines the substance characteristics of nanocomposites in reinforced using straighter and extended BNNT fibers, is one method for estimating the parameters of the nanotechnology plate. This fiber requires that its stiffness constants are expressed in the following order when dispersed in the polymer nanocomposites isotropic in nature matrix.

$$F_{11} = \eta_1 U_{BNNT} F_{11}^{BNNT} + U_n F^n \tag{42}$$

$$\frac{\eta_2}{F_{22}} = \frac{U_{BNNT}}{F_{22}^{BNNT}} + \frac{U_n}{F^n} \tag{43}$$

$$\frac{\eta_3}{H_{12}} = \frac{U_{BNNT}}{H_{12}^{BNNT}} + \frac{U_n}{F^n} \tag{44}$$

Furthermore, the amount of portions of the matrix material and BNNTs are represented by $U_n$andU_{BNNT}, correspondingly.

$$U_{BNNT} + U_n = 1 \tag{45}$$

The expressions for the thermal contraction factors are

$$\alpha_{11} = U_{BNNT}\alpha_{11}^{BNNT} + U_n\alpha^n \quad (46)$$

$$\alpha_{22} = \left(1 + u_{12}^{CNT}\right)U_{BNNT}\alpha_{11}^{BNNT} + (1 + u^n)U_n\alpha^n - u_{12}\alpha_{11} \quad (47)$$

Where

$$u_{12} = U_{BNNT}u_{12}^{CNT} + U_n u^n \quad (48)$$

The structural reaction during free vibration is complicated by the micro beams' fractures. The main focus of the study is how the peculiar qualities of BNNTs affect the composite's resistance to vibration and how it reacts to it, particularly when fractures are present. The gradient of BNNT concentration, crack size, and dispersion are expected to be important factors in defining the FG-BNNTRC's overall performance.

IV. Result and discussion

The results demonstrate the complex interactions between nanoscale reinforcements and structural integrity by revealing appreciable variations in vibration frequencies. The study highlights that the length scale, length thickness ratio, and volume percentage are some of the elements that significantly affect the frequencies.

IV.i. Temperature variation of a nanocomposite panel reinforced with Functionally Graded Boron Nitride Nanotube-Reinforced Composite (FG-BNNTRC)

A panel of nanocomposite reinforced with boron nitride nanotubes is said to respond differently to temperature variations in terms of temperature variation. A nanocomposite panel is defined as a material consisting of a polymer matrix reinforced with cylindrical boron nitride nanotubes a combination of boron and nitrogen atoms. Its mechanical and thermal properties are improved by the incorporation of nanotubes in the composite. The distinct characteristics of boron nitride nanotubes affect the way the material acts, which is subject to thermal expansion or contraction when the panel's temperature varies. Figure 2 depicts how different b/g affect the temperature field in relation tob/g. In addition to larger piezoelectric plates and higherk/g, the required temperature field rises, as this figure illustrates. Furthermore, whileb/gincreases the curves' slopes drop and the variance between different k/gincreases. The high$k/g$the essential temperature field of the stronger plate results in an increase in the double-bounded nanocomposite thermoelectric plate reinforced by BNNT.

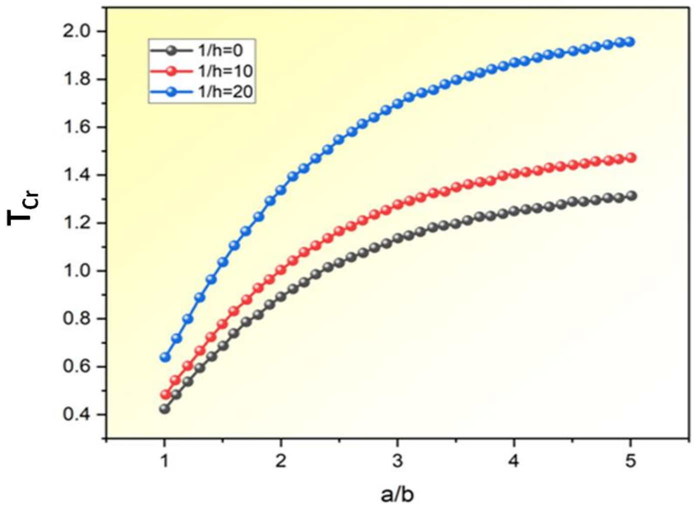

Fig. 2. The temperature change of aFG-BNNTRC at different length-to-thickness ratios

IV.ii. A comparison between the four frequencies and the crack position

According to the Euler-Bernoulli model, modifying the distribution of pair stresses under varied edge crack locations, various crack severity levels K, varying PR, and the substance dimension variable, the findings shown in this portion represent the typical frequencies of microbeams. The results displayed in Table 1 have been compared to four oscillations and fractures located at$\xi = 0.25$. Consider the inertia of rotation is disregarded, along with PR, and a variable for this result is obtained by setting the radial dimension of the component to zero.

Table 1: An examination of the four frequencies in relation to the crack situated at $\xi = 0.25$

λ	Present Values (K)	Present values (K)	Present values (K)	Present values (K)
	0	**.065**	**.35**	**2**
1	3.50	3.10	2.92	2.36
2	6.32	6.12	5.66	5.14
3	9.53	9.32	9.10	8.91
4	12.69	12.65	12.60	12.62

According to the Euler-Bernoulli model, modifying the distribution of couple stresses for different edge fracture locations, variations in crack severity K, variations in PR, and the substance dimension variable, the findings shown in this portion represent the typical frequencies of microbeams. The results displayed in Table 2 have been compared to four frequencies and the crack located at$\xi = 0.50$. Considering the inertia of rotation is disregarded, to achieve this outcome; the substance length scale factor has been configured to 0.

Table 2: Examining the four frequencies in relation to the $\xi = 0.50$

λ	Present Values (K)	Present values (K)	Present values (K)	Present values (K)
	0	**.065**	**.35**	**2**
1	3.15	3.07	2.76	2.10
2	6.30	6.29	6.29	6.29
3	9.44	9.17	8.63	8.10
4	12.57	12.60	12.60	12.56

IV.iii. Initial four inherent resonances featuring a crack at n = 0.25 and n = 0.50 for η

Additionally, the beam's breadth (b = 10 h) and length (L = 100 h) are chosen to examine the four natural frequencies. To investigate the impact of the material length scale parameter l on the natural frequencies, another dimension-free parameter, $\eta = \mathrm{h}/l$, the scaling parameter, which is the relationship between beam height and material length is introduced. The first four frequencies are computed using the values found in Table 3 for different fracture severities, PR, varied parameterη, and crack placements. It is evident that when crack severity grows, the first four frequencies gradually decrease. Additionally, it is clear, that when the microbeams are$\xi = 0.25$, the fourth natural frequency remains constant for a range of PR and crack severities. Furthermore, a positive correlation between the total number of frequencies and the rising PR is discovered. Table 4 shows the microbeams are$\xi = 0.50$, there is no change to the fourth natural frequency for a range of PR and crack severities.

Table 3: Initial 4 natural frequency including a fissure at $\xi = 0.50$ and $\eta = 1$

K	1st$\bar{\Omega}$	2nd$\bar{\Omega}$	3rd$\bar{\Omega}$	4th$\bar{\Omega}$	1st$\bar{\Omega}$	2nd$\bar{\Omega}$	3rd$\bar{\Omega}$	4th$\bar{\Omega}$
	u=.28				**u= .30**			
0.0	4.33394	8.66734	12.9997	17.3304	4.34339	8.68624	13.028	17.3682
0.065	4.20332	8.66734	12.6442	17.3304	4.21249	8.68624	12.6718	17.3682
0.35	3.79317	8.66734	11.8805	17.3304	3.80143	8.68624	11.9064	17.3682
2.0	2.89153	8.66734	11.1361	17.3304	2.89783	8.68624	11.1604	17.3682
K	**u = .33**				**u=.38**			
0.0	4.36797	8.73541	13.1018	17.4665	4.45548	8.91041	13.3642	17.8164
0.065	4.23633	8.73541	12.7435	17.4665	4.3212	8.91041	12.9988	17.8164
0.35	3.82295	8.73541	11.9738	17.4665	3.89954	8.91041	12.2137	17.8164
2.0	2.91424	8.73541	11.2236	17.4665	2.97262	8.91041	11.4484	17.8164

Table 4:The initial 4 natural frequencies have a fissure located at $\xi = 0.25$ and $\eta = 1$

K	1st$\bar{\Omega}$	2nd$\bar{\Omega}$	3rd$\bar{\Omega}$	4th$\bar{\Omega}$	1st$\bar{\Omega}$	2nd$\bar{\Omega}$	3rd$\bar{\Omega}$	4th$\bar{\Omega}$
	u=.28				u= .30			
0.0	4.33394	8.66734	12.9997	17.3304	4.34339	8.68624	13.028	17.3682
0.065	4.26565	8.41862	12.8305	17.3304	4.27495	8.43697	12.8585	17.3682
0.35	4.0105	7.79285	12.5199	17.3304	4.01925	7.80984	12.5472	17.3682
2.0	3.24092	7.04198	12.2774	17.3304	3.24799	7.05733	12.3041	17.3682
K	**u= .33**				**u= .38**			
0.0	4.36797	8.73541	13.1018	17.4665	4.45548	8.91041	13.3642	17.8164
0.065	4.29915	8.48473	12.9313	17.4665	4.38527	8.65471	13.1903	17.8164
0.35	4.0420	7.85405	12.6182	17.4665	4.12297	8.01139	12.8710	17.8164
2.0	3.26637	7.09728	12.3738	17.4665	3.33181	7.23947	12.6217	17.8164

IV.iv. PR for various levels of cracking severity

The findings of the investigation examine the effects concerning the initial fracture location, spatial scaling length variable, and PR natural frequency. Furthermore, a correlation between the crack's quality characteristic and its inherent rate has been found to significantly decreases. In addition, it becomes evident whenever the fracture severity metric quadruples, the natural frequency is nearly twice as high. Furthermore, without dimension materials, the inherent frequency grows as the length scale variable decreases significantly, as shown in Figures 3 and 4. The natural frequency decreases by half as the severity of the cracks increases four times. A cracked $\xi = 0.50$ has a far lower total natural frequency than one cracked at$\xi = 0.25$.

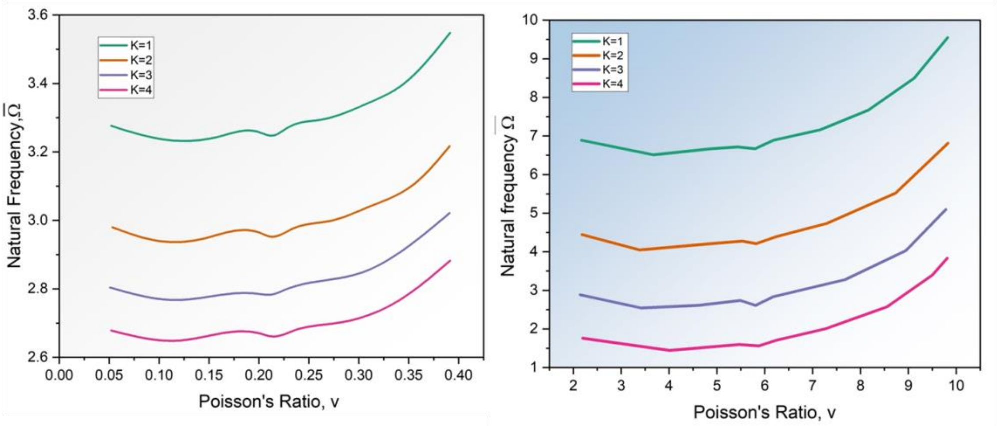

Fig. 3. PR for different crack severity at $\xi = 0.50$

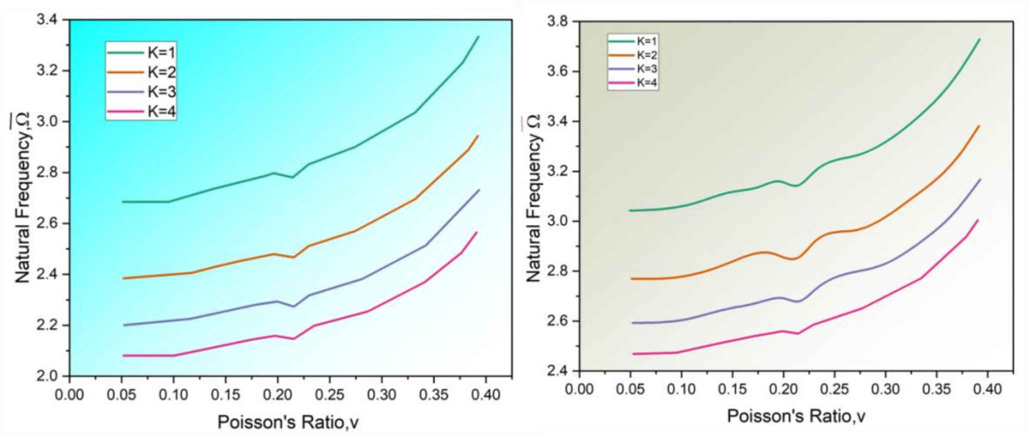

Fig. 4. PR for different crack severity at $\xi = 0.25$

IV.v. Effect of crack position for diverse η

The impact of fracture position on natural frequency is depicted in Figure 5. It goes without saying that the conventional wisdom was the natural frequency would exhibit as relocating the crack from one beam edge to the other, periodic variations other because of the balanced barrier constraints that the microbeams had to overcome. Furthermore, it demonstrated that the location of the fracture in the center of the microbeams represents the smallest amount of natural frequency. Furthermore, the values greater than 4, there is a minimal impact of the dimensionless material length scale parameter on natural frequencies.

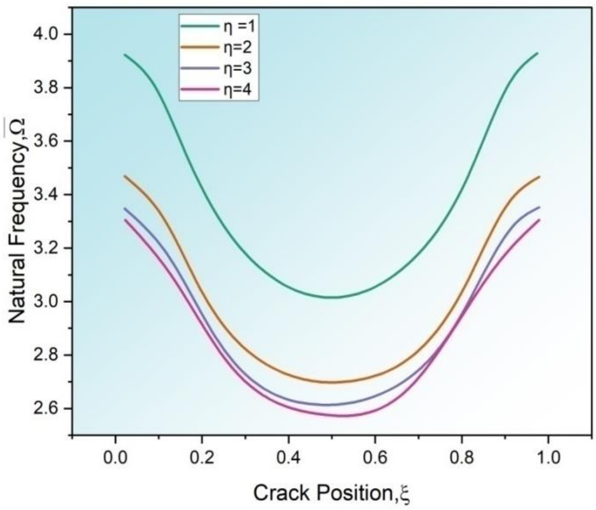

Figure 5: Natural frequencies are essentially unaffected by the crack position for different η when $v = .3$ and $K = 1.5$

IV.vi. Effect of crack position for diverse u

PR significantly affects the crack position and natural frequency, as seen by the results displayed in Figure 6. It has been proven that the inherent frequencies essentially stay the same for microbeams with a PR of .15 to .35. Since as long as it is greater than 0.35, it rises significantly.

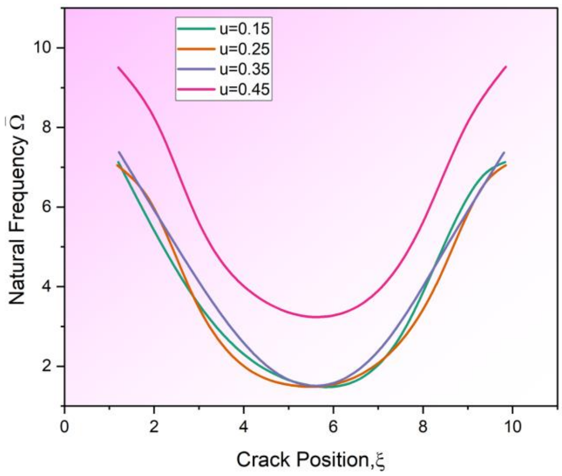

Fig. 6. Effect of fracture position on inherent frequencies for different u when $K = 1.5$ and $\eta = 1$

IV.vii. Discussion

The effects of material length scale, fracture position, and PR on natural frequencies are investigated. As crack severity increases, the results show a progressive decline in frequencies, highlighting the complex interactions among these variables. The outcomes, show how natural frequencies are affected by fracture position, material length scale, and PR. The study focuses attention on expected results, including the strong effect of PR on natural frequencies and the asymmetric fluctuation of natural frequencies with different fracture positions. The comprehensive analysis clarifies the complex linkages controlling the natural frequencies of microbeams with edge fractures as well as the diverse behaviors of a nanocomposite panel under temperature fluctuations. Future research in structural mechanics and nanocomposite materials will benefit from the nuanced understanding of the examined phenomena provided by the data and visualizations offered. The mechanical strength and stiffness of the composite matrix are enhanced by the addition of FG-BNNTRC. Renowned for its remarkable mechanical characteristics, FG-BNNTRC enhances and improves the composite material's overall structural integrity.

V. Conclusion

The study analyzes the size-dependent vibration of cracked micro beams with FG-BNNTRC using the Euler-Bernoulli beam theory and the MCS theory. The effects on the natural frequencies of the following factors: Factors such as PR, fracture location, crack severity, and dimensions of the material scale. A negative correlation has been seen between the crack severity and natural frequencies. A major factor influencing natural frequency is crack severity. The break advances towards the center of the beam, causing a fall in natural frequency overall. The findings have important ramifications for the creation of novel composite materials for use in micro-scale applications. Expanding our knowledge of material behavior in micro-electromechanical systems is made possible by the investigation of the intricate relationships between structural integrity and nanoscale reinforcements. The study makes novel approaches to the optimization and design of micro-scale structures applicable to a variety of technical domains and advances the larger objective of using Functionally Graded Boron Nitride Nanotube-Reinforced Composite (FG-BNNTRC)to improve the mechanical performance of composite materials.

Conflict of Interest:

There is no conflict of interest regarding this paper.

References

I. Arshid, Ehsan, and Saeed Amir. "Size-dependent vibration analysis of fluid-infiltrated porous curved microbeams integrated with reinforced functionally graded graphene platelets face sheets considering thickness stretching effect." *Proceedings of the Institution of Mechanical Engineers, Part L: Journal of Materials: Design and Applications* 235, no. 5 (2021): 1077-1099.

II. Bakhtiari-Nejad, F. and Nazemizadeh, M., 2016. Size-dependent dynamic modeling and vibration analysis of MEMS/NEMS-based nanomechanical beam based on the nonlocal elasticity theory. *Acta Mechanica*, *227*(5), pp.1363-1379.

III. Chen, D., Zheng, S., Wang, Y., Yang, L. and Li, Z., 2020. Nonlinear free vibration analysis of a rotating two-dimensional functionally graded porous micro-beam using isogeometric analysis. *European Journal of Mechanics-A/Solids*, *84*, p.104083.

IV. Civalek, Ö., Akbaş, Ş.D., Akgöz, B. and Dastjerdi, S., 2021. Forced vibration analysis of composite beams reinforced by carbon nanotubes. Nanomaterials, 11(3), p.571.

V. Eghbali, M., Hosseini, S.A. and Pourseifi, M., 2022. Free transverse vibrations analysis of size-dependent cracked piezoelectric nano-beam based on the strain gradient theory under mechanic-electro forces. *Engineering Analysis with Boundary Elements*, *143*, pp.606-612.

VI. Guo, L.J., Mao, J.J., Zhang, W. and Wu, M., 2023. Stability Analyses of Cracked Functionally Graded Graphene-Platelets Reinforced Composite Beam Covered with Piezoelectric Layers. *International Journal of Structural Stability and Dynamics*, p.2350164.

VII. Heo, J., Yang, Z., Xia, W., Oterkus, S. and Oterkus, E., 2020. Free vibration analysis of cracked plates using peridynamics. *Ships and Offshore Structures*, *15*(sup1), pp.S220-S229.

VIII. Huang, T., Li, Y., Chen, M. and Wu, L., 2020. Bi-directional high thermal conductive epoxy composites with radially aligned boron nitride nanosheets lamellae. *Composites Science and Technology*, *198*, p.108322.

IX. Jones, R.S., Gonzalez-Munoz, S., Griffiths, I., Holdway, P., Evers, K., Luanwuthi, S., Maciejewska, B.M., Kolosov, O. and Grobert, N., 2023. Thermal Conductivity of Carbon/Boron Nitride Heteronanotube and Boron Nitride Nanotube Buckypapers: Implications for Thermal Management Composites. *ACS Applied Nano Materials*.

X. Ko, J., Kim, D., Sim, G., Moon, S.Y., Lee, S.S., Jang, S.G., Ahn, S., Im, S.G. and Joo, Y., 2023. Scalable, Highly Pure, and Diameter-Sorted Boron Nitride Nanotube by Aqueous Polymer Two-Phase Extraction. *Small Methods*, *7*(4), p.2201341.

XI. Kumar, M. and Sarangi, S.K., 2022. Bending and vibration study of carbon nanotubes reinforced functionally graded smart composite beams. Engineering Research Express, 4(2), p.025043.

XII. Larkin, K., 2020. *Nonlinear Size Dependent Analysis and Crack Network Modeling of Micro/Nano-systems* (Doctoral dissertation, New Mexico State University).

XIII. Mercan, K. and Civalek, Ö., 2022. Comparative Stability Analysis of Boron Nitride Nanotube using MD Simulation and Nonlocal Elasticity Theory. International Journal of Engineering and Applied Sciences, 13(4), pp.189-200.

XIV. Numanoğlu, H.M. and Civalek, Ö., 2022. Novel size-dependent finite element formulation for modal analysis of cracked nanorods. *Materials Today Communications*, *31*, p.103545.

XV. Rahi, A., 2018. Crack mathematical modeling to study the vibration analysis of cracked micro beams based on the MCST. *Microsystem Technologies*, *24*(7), pp.3201-3215.

XVI. Sahmani, S. and Safaei, B., 2019. Nonlinear free vibrations of bi-directional functionally graded micro/nano-beams including nonlocal stress and microstructural strain gradient size effects. *Thin-Walled Structures*, *140*, pp.342-356.

XVII. Sedighi, H.M., Malikan, M., Valipour, A. and Żur, K.K., 2020. Nonlocal vibration of carbon/boron-nitride nano-hetero-structure in thermal and magnetic fields by means of nonlinear finite element method. *Journal of Computational Design and Engineering*, *7*(5), pp.591-602.

XVIII. Shafiei, H. and Setoodeh, A.R., 2020. An analytical study on the nonlinear forced vibration of functionally graded carbon nanotube-reinforced composite beams on nonlinear viscoelastic foundation. *Arch. Mech*, *72*(2), pp.81-107.

XIX. Sh Khoram-Nejad, E., Moradi, S. and Shishesaz, M., 2021. Free vibration analysis of the cracked post-buckled axially functionally graded beam under compressive load. *Journal of Computational Applied Mechanics*, *52*(2), pp.256-270.

XX. Song, M., Gong, Y., Yang, J., Zhu, W. and Kitipornchai, S., 2020. Nonlinear free vibration of cracked functionally graded graphene platelet-reinforced nanocomposite beams in thermal environments. *Journal of Sound and Vibration*, *468*, p.115115.

XXI. Vandecruys, E., Van de Velde, M., Reynders, E., Lombaert, G. and Verstrynge, E., 2023. Experimental study on acoustic emission sensing and vibration monitoring of corroding reinforced concrete beams. *Engineering Structures*, *293,* p.116553.

XXII. Xu, C., Rong, D., Zhou, Z., Deng, Z. and Lim, C.W., 2020. Vibration and buckling characteristics of cracked natural fiber reinforced composite plates with corner point-supports. *Engineering Structures*, *214*, p.110614.

XXIII. Yan, J.W. , He, J.B. and Tong, L.H., 2019. Longitudinal and torsional vibration characteristics of boron nitride nanotubes. *Journal of Vibration Engineering & Technologies*, *7*, pp. 205-215.

XXIV. Zeighampour, H., Tadi Beni, Y. and Kiani, Y., 2020. Electric field effects on buckling analysis of boron–nitride nanotubes using surface elasticity theory. *International Journal of Structural Stability and Dynamics*, *20* (12), p.2050137.

XXV. Zeighampour, H. and Tadi Beni, Y., 2020. Buckling analysis of boron nitride nanotube with and without defect using molecular dynamic simulation. Molecular Simulation, 46(4), pp.279-288.

XXVI. Zhao, J.L., Chen, X., She, G.L., Jing, Y., Bai, R.Q., Yi, J., Pu, H.Y. and Luo, J., 2022. Vibration characteristics of functionally graded carbon nanotube-reinforced composite double-beams in thermal environments. Steel Compos Struct, 43(6), pp.797-808.

XXVII. Zhu, L.F., Ke, L.L., Xiang, Y., Zhu, X.Q. and Wang, Y.S., 2020. Vibrational power flow analysis of cracked functionally graded beams. *Thin-Walled Structures*, *150*, p.106626.